# An on-chip fully electronic molecular clock based on sub-terahertz rotational spectroscopy

Cheng Wang<sup>®</sup>, Xiang Yi, James Mawdsley<sup>®</sup>, Mina Kim, Zihan Wang and Ruonan Han<sup>®</sup>\*

Mobile electronic devices require stable, portable and energy-efficient frequency references (or clocks). However, current approaches using quartz-crystal and microelectromechanical oscillators suffer from frequency drift. Recent advances in chipscale atomic clocks, which probe the hyperfine transitions of evaporated alkali atoms, have led to devices that can overcome this issue, but their complex construction, cost and power consumption limit their broader deployment. Here we show that sub-terahertz rotational transitions of polar gaseous molecules can be used as frequency bases to create low-cost, low-power miniaturized clocks. We report two molecular clocks probing carbonyl sulfide (16012C32S), which are based on laboratory-scale instruments and complementary metal-oxide-semiconductor chips. Compared with chip-scale atomic clocks, our approach is less sensitive to external influences and offers faster frequency error compensation, and, by eliminating the need for alkali metal evaporation, it offers faster start-up times and lower power consumption. Our work demonstrates the feasibility of monolithic integration of atomic-clock-grade frequency references in mainstream silicon-chip systems.

ighly stable clocks are critical for electronic systems in navigation, communication and sensing applications<sup>1</sup>. For portable equipment under GPS-denied conditions (such as underwater sensors), additional clock features, for example compactness and high energy efficiency, also become indispensable. Widely adopted oscillators based on quartz crystal<sup>2</sup> and microelectromechanical system (MEMS) resonators<sup>3</sup> suffer from frequency drift caused by aging and disturbances from the environment such as temperature variation and mechanical vibration. This leads to long-term clock stability worse than the parts-per-billion (10<sup>-9</sup>) level.

Previously, outstanding long-term stability has been achieved in atomic clocks<sup>1,4-6</sup> by referencing to the electron transition frequencies of atoms. However, most of these clocks are bulky and power consuming. Using optical coherent population trapping (CPT)<sup>7-10</sup>, chip-scale atomic clocks (CSACs)<sup>11-15</sup> have been successfully miniaturized. For example, the SA.45s CSAC12,16 achieves a frequency stability (expressed as Allan deviation<sup>17</sup>,  $\sigma_v$ ) of  $3.0 \times 10^{-10}$ for a short-term averaging time  $\tau = 1$  s and  $\sim 1 \times 10^{-11}$  for a longterm averaging time of  $\tau = 1,000 \,\mathrm{s}$  to one day, and it consumes a d.c. power of 120 mW and occupies a volume of 16 cm<sup>3</sup>. However, the complicated (hence high-cost) assembly of their electro-optical components limits their application. The hyperfine transition used in these clocks is also sensitive to external electric/magnetic fields, which therefore necessitates dedicated shielding around the alkali gas cell. Another disadvantage of the technology is the long startup time (~2 min; refs 12,16) required by the alkali-metal evaporation and related thermal stabilization. Finally, the narrow bandwidth (and hence slow response time) of the servo loop in a CSAC, limited by the kilohertz-level transition linewidth, degrades the correction speed for frequency deviations caused by, for example, mechanical vibrations<sup>18</sup>.

Clocks based on fully-electronic spectroscopic probing of gas molecules are expected to have significantly simplified, heater-free implementations (hence low cost and faster start-up). To this end, the inversion spectrum of ammonia (NH<sub>3</sub>) at  $\sim$ 23.8 GHz was exploited as a source of clock reference<sup>5,19–24</sup>. The inversion of ammonia is a vibrational motion, in which the nitrogen atom

tunnels through the plane of three hydrogen atoms<sup>25</sup>. In 1977, an Allan deviation of  $2 \times 10^{-10}$  for  $\tau = 1,000 \, \mathrm{s}$  was reported from an ammonia  $\mathrm{clock}^{24,26}$ . However, due to the large size of the gas cell waveguide ( $\sim 1-2$  l), which is limited by the large wavelength and weak absorption, miniaturization of ammonia clocks is not feasible.

In this Article, we report the use of a new physical mechanism the rotational spectrum of gaseous linear molecules (carbonyl sulfide, <sup>16</sup>O<sup>12</sup>C<sup>32</sup>S (OCS), is specifically used in this work) in the sub-terahertz range (~200-300 GHz)—as a clock reference. A key trend that has led us to this approach is that spectroscopic detection in this sub-terahertz regime is achievable with electronics and has also recently been demonstrated using integrated circuits with mainstream complementary metal-oxide-semiconductor (CMOS) technologies<sup>27</sup>. This opens up opportunities to develop chip-scale clocks with low cost and power. Compared to caesium and rubidium, OCS is chemically stable<sup>28</sup>, and its rotational spectral lines are more robust under external electric/magnetic fields. For example, it has a low g factor of 0.03 (ref. 29) as opposed to 2 in caesium clocks. This, along with its ~30 times higher probing frequency, leads to a greatly reduced relative drift as a result of the Zeeman effect. Compared to ammonia clocks, the OCS spectral lines used in our approach have a higher quality factor and much greater absorption intensity, enhancing the short-term stability. In addition, because of the much smaller wavelength of the subterahertz signal, the volume of the gas cell can be reduced to the level of cm<sup>3</sup>, allowing clock miniaturization. We report here experimental studies for the rotational spectrum of OCS, and demonstrate two clock prototypes. The first is a laboratory-scale, instrument-based prototype that uses a high-order harmonic dispersion curve of the molecular spectrum and achieves a measured Allan deviation that is comparable with CSACs (up to  $\tau = 1,000 \text{ s}$ ) and 10 times better than an ammonia clock. The second is a chipscale molecular clock using a standard 65 nm CMOS process, which consumes only 66 mW of d.c. power. Because OCS maintains the gas phase above -50 °C and has a 1,000 times larger linewidth than that of CSAC, both prototypes also demonstrate fast start-up and frequency-compensation operations.

ARTICLES NATURE ELECTRONICS

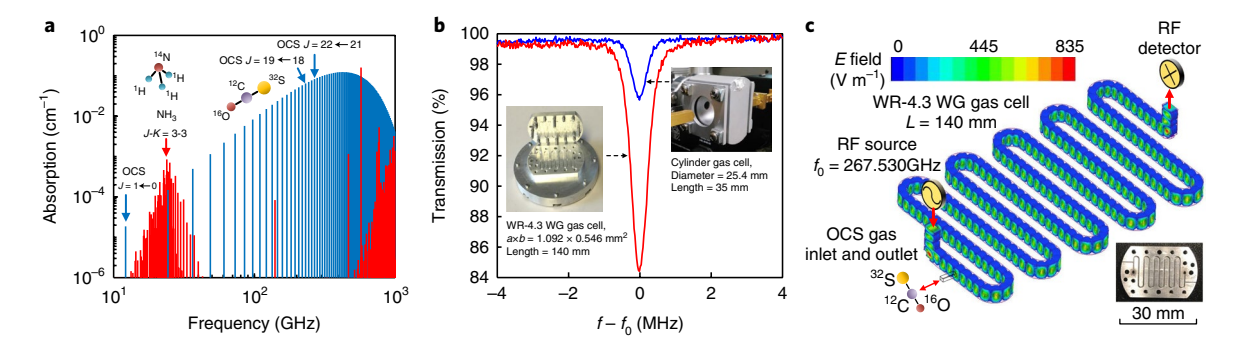


**Fig. 1 | Rotational spectrum of OCS in a WR-4.3 waveguide gas cell. a**, Calculated absorption coefficient within  $\sim$ 0.1–1 THz of carbonyl sulfide ( $^{16}O^{12}C^{32}S$ , blue) and ammonia ( $^{14}N^{1}H_{3}$ , red) under a pressure of 10 Pa (ref.  $^{39}$ ). **b**, Measured Doppler-limited linewidth of OCS at  $f_0 = 267.530239$  GHz using a cylinder gas cell (FWHM = 573 kHz) and a WR-4.3 rectangular waveguide gas cell (FWHM = 573 kHz) under a pressure of 1Pa and radiofrequency (RF) power of 1 $\mu$ W. **c**, Simulated electric field distribution of WR-4.3 rectangular waveguide gas cell at  $f_0$ . The injected RF power is 0.1 mW.

# Sub-terahertz rotational spectrum of OCS

The rotational behaviour of linear molecules such as OCS is guantized (quantum number I), and the related absorption spectrum consists of a set of equally spaced lines (spacing of ~12.16 GHz for OCS)<sup>25</sup>. For the transition from I to I+1, on the one hand each J state has 2J+1 degenerated sublevels, so the total available levels increases with J; on the other hand, due to the Boltzmann distribution, the probability of a state being occupied by a molecule decreases exponentially with increasing state energy (larger J). As a result, as shown in Fig. 1a, the absorption intensity of the OCS rotation spectrum reaches its peak in the sub-terahertz regime. Specifically, the absorption of the 267.530 GHz spectral line  $(J=22\leftarrow21)$  of OCS is 4,440 times higher than that at 12.16 GHz ( $I=1\leftarrow0$ ), and 98 times higher than the aforementioned ammonia line at 23.8 GHz. The intensive absorption of OCS lines in the sub-terahertz range improves the signal-to-noise ratio (SNR) and hence the short-term stability of the clock, which is determined by the product of the SNR and the quality factor Q of the detected spectral line<sup>30</sup>.

We experimentally studied the following spectral-broadening mechanisms, where the quality factor Q is defined as the ratio between the centre frequency ( $f_0 = 267.530 \,\text{GHz}$  for the tested line) and the full-width at half-maximum (FWHM). (1) Under low pressure, the linewidth is broadened by the Doppler effect from the Brownian motion of molecules (Doppler broadening)<sup>25</sup>. Using a cylindrical gas cell with a diameter of 25.4 mm, we obtained a Doppler-limited linewidth of  $\Delta v_1 = 534 \,\mathrm{kHz}$  ( $Q = 5.0 \times 10^5$ ) at 300 K (Fig. 1b). In contrast, NH<sub>3</sub> has a 50% lower Doppler-limited Q due to its lighter molecule weight. (2) When the gas cell is miniaturized to a single-mode waveguide, the more frequent collisions between OCS molecules and the gas cell wall contribute additional linewidth  $\Delta v_2$  (wall broadening). To study this, a metallic single-mode waveguide was fabricated that had crosssectional dimensions of 1.092 × 0.546 mm<sup>2</sup> (WR-4.3) and a length of 14cm (Fig. 1c). The waveguide has a meandering geometry for small gas cell size. Figure 1b shows that at 1 Pa the wall collision broadens the total linewidth to  $(\Delta v_1^2 + \Delta v_2^2)^{1/2} = 573 \,\text{kHz}$  $(Q=4.7\times10^5)$ . Although the gas cell dimension is comparable to the mean free path of OCS ( $\lambda_0 \approx 0.9$  mm at 1 Pa), the Doppler effect is still dominant. (3) Under high pressure and reduced lifetime by intermolecular collisions, the total FWHM becomes limited by the pressure-broadened linewidth  $\Delta v_3$ . Related measurement results with the WR-4.3 waveguide gas cell, which are presented in Fig. 2a and summarized in Fig. 2b, show that pressure-induced broadening becomes dominant over Doppler broadening and wall broadening above  $\sim$ 5 Pa. (4) Finally, when large incident power induces transitions at a rate that is not negligible compared with the collision rate, thermal equilibrium no longer holds. Power saturation and associated linewidth broadening then occur<sup>25,31</sup>. As shown in

Fig. 2d,e, beyond an RF power of  $\sim 10\,\mu\text{W}$ , the relative absorption decreases along with line broadening due to this saturation.

Based on these data, the predicted short-term Allan deviation  $(\tau=1\,\mathrm{s})$  of an OCS clock is presented in Fig. 2c,f. This is based on equation (1) (see next section). State-of-the-art sensitivities of CMOS square-law detectors (using a Schottky barrier diode or field-effect transistor) and CMOS heterodyne receivers (using a frequency mixer driven by a local oscillator coherent with the probing signal) are assumed, and other SNR-degrading factors, such as sub-terahertz signal phase noise and coupling/transmission loss, are not included. We show that, using CMOS technology, a short-term  $(\tau=1\,\mathrm{s})$  stability near  $10^{-12}$  can be achieved via heterodyne detection. The associated pressure and signal power conditions are  $\sim 5\,\mathrm{Pa}$  and  $\sim 60\,\mu\mathrm{W}$ .

### Laboratory-scale molecular clock

A photograph and schematic of the molecular clock are presented in Fig. 3a,b. The sub-terahertz signal is generated by a frequency multiplier chain and detected by a heterodyne receiver; both instruments are fed by a voltage-controlled crystal oscillator (VCXO). Wavelength modulation spectroscopy (WMS)32 was adopted for transmission-mode line probing. As shown in Fig. 3c, the centre frequency  $f_c$  of the sub-terahertz signal varies with modulation frequency  $f_{\rm m}$  and frequency deviation  $\Delta f$ , where  $f_{\rm m} \ll \Delta f$ .  $\Delta f$  is comparable with the FWHM (~1 MHz). When  $f_c \approx f_0$ , the envelope of the received sub-terahertz signal, which is obtained from a diode rectifier, fluctuates periodically at  $f_{\rm m}$  according to the absorptive line profile of OCS. This signal is then detected by a lock-in amplifier at its fundamental and odd harmonic frequencies. By scanning  $f_c$ , spectral curves  $V_r$  derived from the  $f_m$ ,  $3f_m$  and  $5f_m$  components of the above envelope signal are obtained (Fig. 3d). V<sub>r</sub>, which is also the error signal representing the frequency difference  $f_c - f_0$ , is fed back to the VCXO after amplification and low-pass filtering. The openloop gain of the entire system is designed to be sufficiently large to suppress long-term drift caused by any clock component (such as the VCXO and power supply) other than the gas itself. Next, the short-term Allan deviation  $\sigma_{\nu}$  of the molecular clock for averaging time  $\tau$  is expressed as<sup>30</sup>

$$\sigma_{y}(\tau) = \frac{V_{r,n}}{K_{r} \cdot f_{0} \cdot \sqrt{2\tau}} \tag{1}$$

where  $V_{\rm r,n}$  and  $K_{\rm r}$  are the noise and zero-crossing slope of the measured fundamental or harmonic spectral curve (Fig. 3e). When the fundamental dispersion curve is used, equation (1) can also be approximated as  $\sigma_y(\tau) \approx 0.2/({\rm SNR} \times Q \times \sqrt{\tau})$ . Because  $K_{\rm r}$  decreases for higher harmonic order due to the reduction in the signal amplitude,

NATURE ELECTRONICS ARTICLES

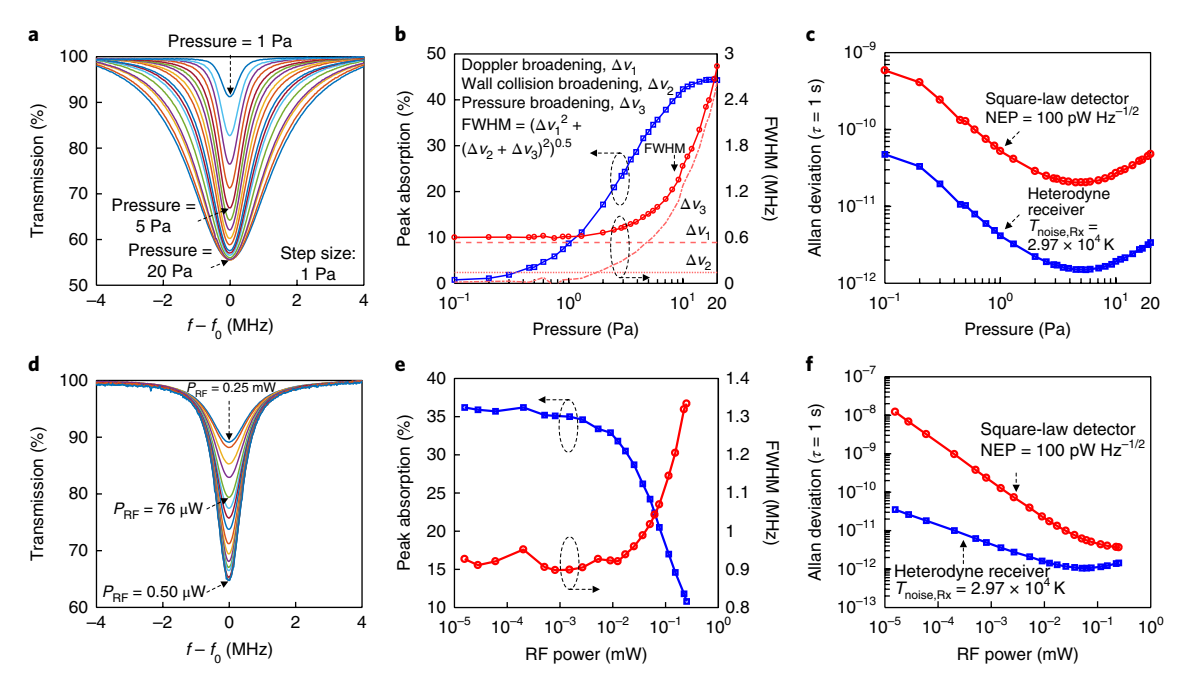


**Fig. 2 | Experimental results and analysis of the OCS spectral line at**  $f_0 = 267.530239$  **GHz. a**, Measured transmission line profile with pressure broadening. **b**, Peak absorption intensity (in percentage) and full-width at half-maximum (FWHM) at different pressures. For **a** and **b**, the injected RF power is 1  $\mu$ W. **c**, Calculated Allan deviation versus pressure with an averaging time  $\tau = 1$  s. **d**, Measured transmission line profile with power saturation broadening. **e**, Peak absorption intensity and FWHM versus RF power. **f**, Calculated Allan deviation versus RF power, with  $\tau = 1$  s. For **d-f**, the assumed OCS pressure is 5 Pa. For **c** and **f**, the assumed noise temperature ( $T_{\text{noise,Rx}}$ ) of the heterodyne receiver is 2.97 × 10<sup>4</sup> K (a noise figure (NF) of 20 dB), and the assumed noise equivalent power (NEP) of the square-law detector is 100 pW Hz<sup>-0.5</sup>.

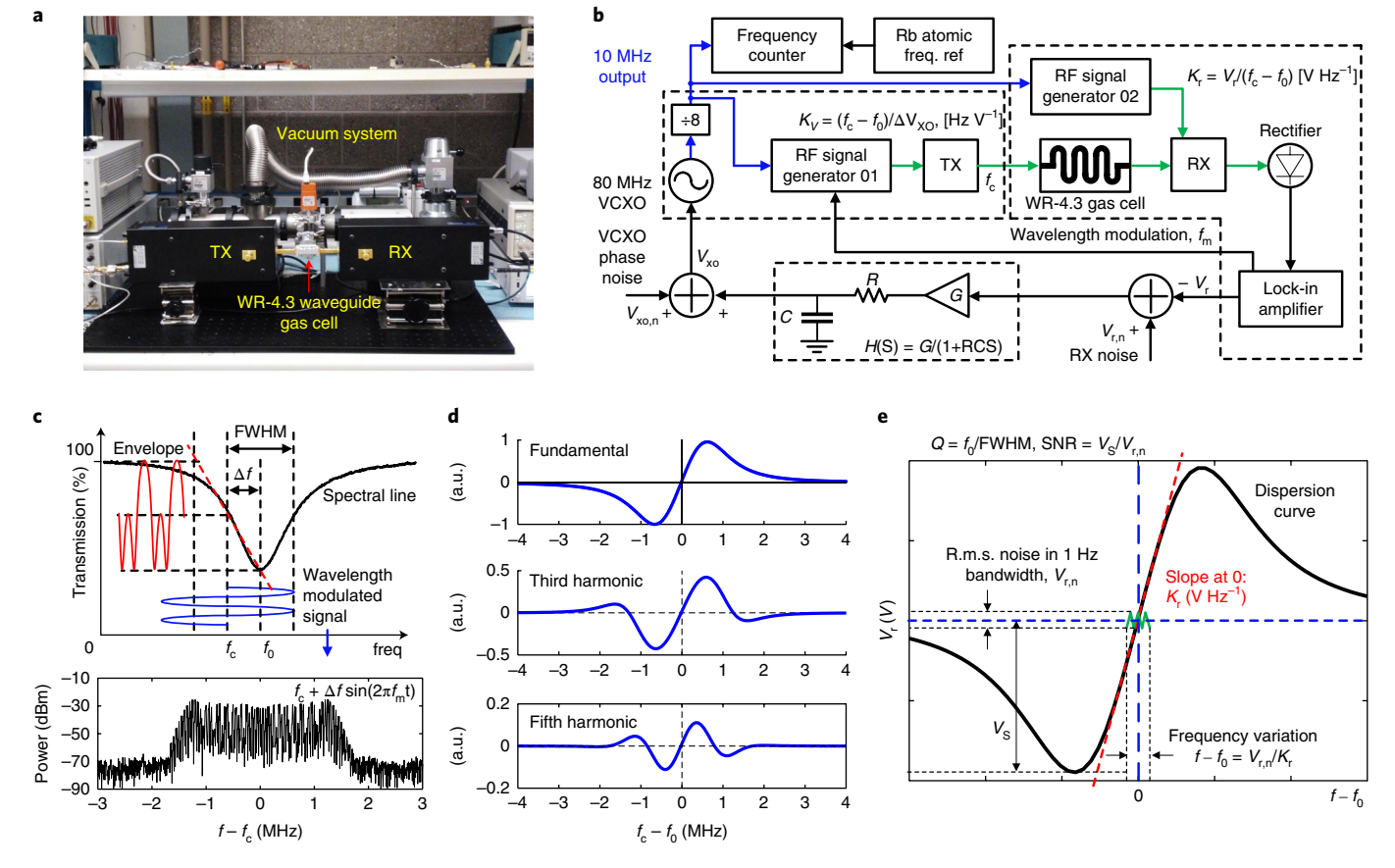


**Fig. 3 | Laboratory-scale molecular clock. a,b**, Photograph and schematic of the laboratory-scale molecular clock. **c**, Probing of the rotational spectral line of OCS ( $f_c$  = 267.530 GHz) using WMS. The spectrum of the sub-terahertz signal is also shown with an RF power of 50 μW, modulation frequency  $f_m$  of 100 kHz and frequency deviation  $\Delta f$  of 1 MHz. **d**, Measured fundamental, third-harmonic and fifth-harmonic dispersion curves of the 267.530 GHz spectral line of OCS. The OCS pressure is 10 Pa. **e**, Frequency variation due to the noise of the dispersion curve.

ARTICLES NATURE ELECTRONICS

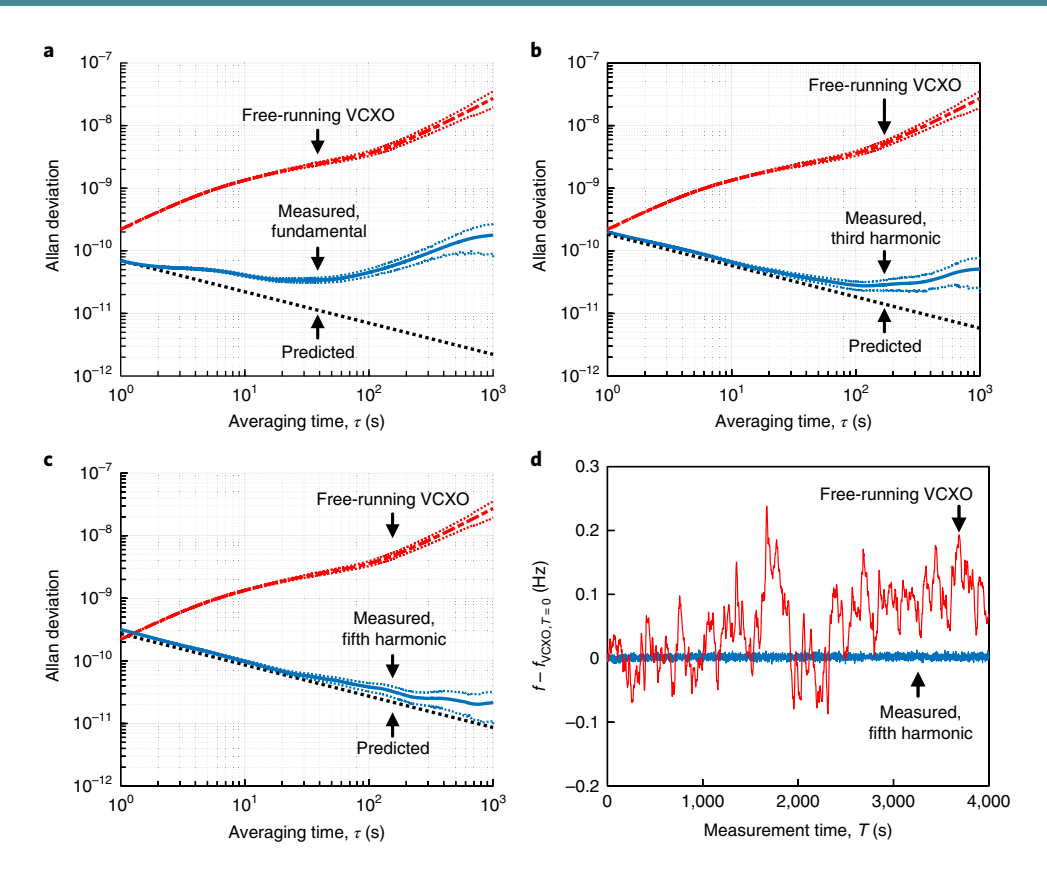


Fig. 4 | Measured stability of the laboratory-scale molecular clock. a-c, Measured overlapping Allan deviations and their confidence intervals for the clock locking to the fundamental, third and fifth harmonic dispersion curves of the 267.530 GHz OCS spectral line, respectively. d, Measured instantaneous frequency of c over 4,000 s. The integration time for each frequency point is 1s.

a molecular clock locking to the fundamental dispersion curve achieves better short-term stability. On the other hand, however, higher harmonic orders suppress the negative impacts introduced by variations in the spectroscopic baseline, and therefore improve the symmetry of the measured curves<sup>24,26</sup>. The baseline variations in the frequency domain are normally caused by standing-wave formations in the gas cell and terahertz transceivers. Compared to the high-Q molecular transition lines, these variations are much more gradual, and thus contain smaller high-order harmonic components. With low-order WMS, the measured curve is asymmetric due to the non-ideal baseline, and its zero-crossing point shifts when the gas pressure changes (due to gas leakage or temperature variation). With high-order WMS, distortion of the baseline superposed on the molecular spectrum is filtered out, so better long-term stability is obtained. Finally, it should be noticed that  $f_m$  is limited by the FWHM because the spectral line can only be probed with a finite speed. An  $f_{\rm m}$  of 100 kHz (or 0.1×FWHM) is chosen for our prototype; this then sets an upper limit for the loop bandwidth because the clock frequency cannot be updated faster than  $f_{\rm m}$ . Thus, the molecular clock is expected to have 1,000 times larger loop bandwidth (or shorter settling time) than CSACs (FWHM  $\approx$  1 kHz). Further details on this topic are provided in the Methods.

In the experiments, an RF power of  $50\,\mu\text{W}$  and OCS pressure of  $10\,\text{Pa}$  were chosen to maximize the short-term stability. The measured FWHM and peak absorption are 1.548 MHz and 36.9%, respectively. The measured SNR with 1 Hz bandwidth for the fundamental, third- and fifth-harmonic dispersion curves (Fig. 3d) are 86.6 dB, 81.4 dB and 71.2 dB, respectively. The measured Allan deviations and instantaneous frequencies with closed-loop locking of the clock are shown in Fig. 4. The measurement time for each curve is  $4,000\,\text{s}$  ( $4\tau_{\text{max}}$ ). Using equation (1), the predicted Allan

deviations based on the measured spectral lines, which incorporate all noise sources, are also plotted. The predicted and measured data agree well in the short-term regime ( $\tau \le 1$  s). For the fundamental, third and fifth harmonics, the Allan deviations  $\sigma_v$  at  $\tau = 1$  s reach  $6.9 \times 10^{-11}$ ,  $2.0 \times 10^{-10}$  and  $3.2 \times 10^{-10}$ , respectively. The measured short-term stability is still inferior to the predictions ( $\sim 1 \times 10^{-12}$ ) in Fig. 2c,f, mainly due to the high noise figure of the receiver and the additional impact of the transmitter phase noise. For long-term stability, the measurement results are also consistent with the earlier explanations that higher harmonic order leads to better long-term stability. The measured  $\sigma_{\nu}$  at  $\tau = 1,000 \,\mathrm{s}$  reaches  $2.2 \times 10^{-11}$  when using the fifth harmonic. In our current prototype, a leakage rate of  $\sim 0.1 \,\mathrm{Pa}\,\mathrm{h}^{-1}$  is observed from the gas cell, which is attributed to the long-term frequency drift of the clock. Additional analyses of long-term stability and the pressure dependency, Stark effect and Zeeman effect are included in the Methods.

# Chip-scale molecular clock on silicon

The fully-electronic operation of our molecular clock makes it possible to realize all clock components other than the gas cell within a chip-scale circuit system. Implementing such systems using main-stream silicon CMOS technology is of particular interest, because it allows low-cost, monolithic integration of an atomic-clock-grade frequency reference into an electronic system-on-chip. To this end, we demonstrate the first chip-scale molecular clock using a standard 65 nm low-power CMOS process<sup>33</sup>. The circuit schematic and the packaged module of the clock are shown in Fig. 5a,b. Figure 5c presents photographs of the transmitter (Tx) and receiver (Rx) parts of the clock, which are implemented in two separate chips with a total area of only 2.4 mm<sup>2</sup>. The separation is to avoid any undesired coupling of sub-terahertz signal through the silicon

NATURE ELECTRONICS ARTICLES

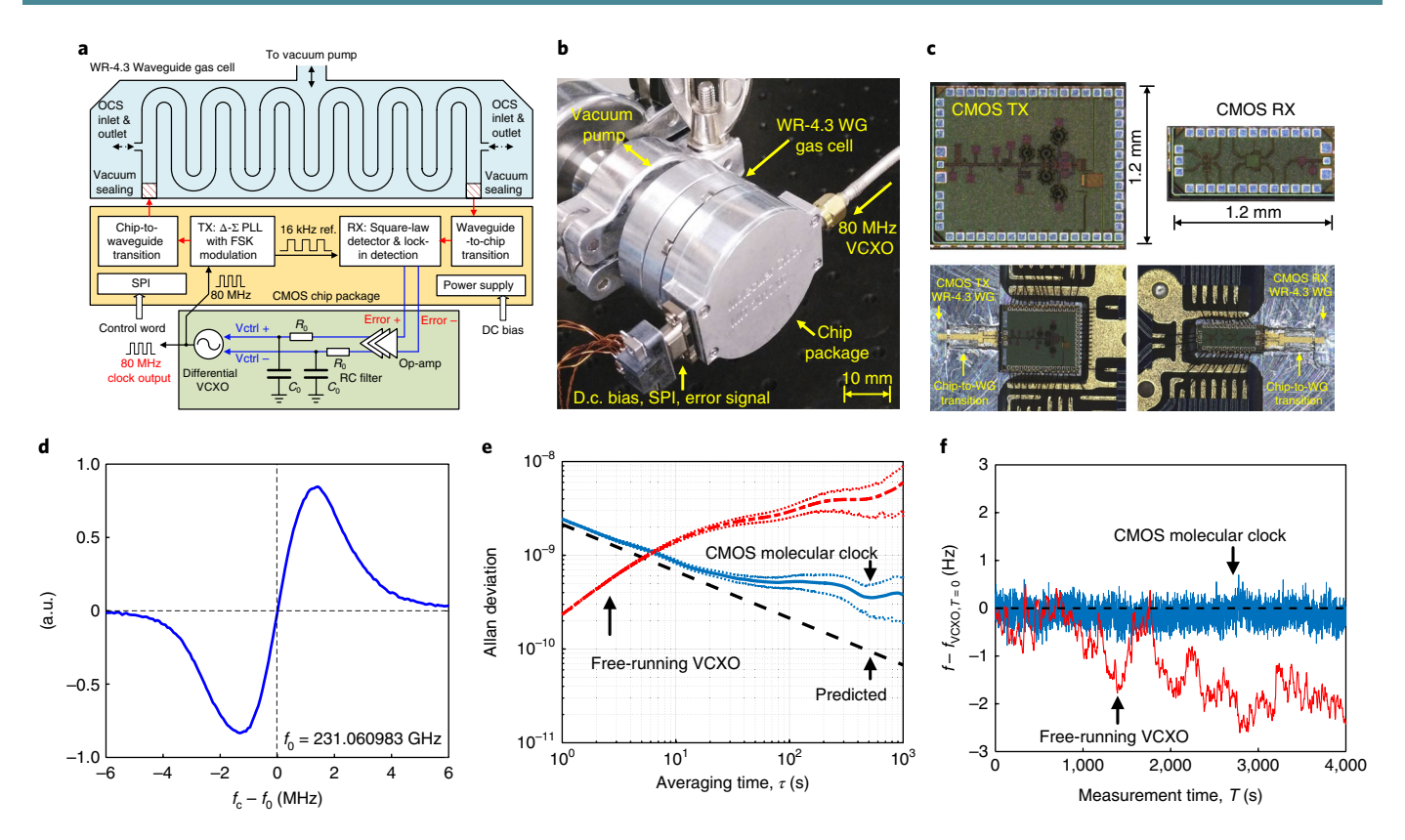


**Fig. 5 | Chip-scale molecular clock on silicon and the measurement results. a,b**, Schematic and photograph of the CMOS molecular clock. **c**, Photographs of the CMOS Tx and Rx chips with wire-bonding and chip-to-waveguide transitions. **d**, Fundamental dispersion curve (FSK,  $f_m = 16$  kHz,  $\Delta f = 1$  MHz) of the 231.061 GHz spectral line of OCS measured by the CMOS molecular clock. **e**, Measured overlapping Allan deviation and confidence interval of the CMOS molecular clock. **f**, Instantaneous frequency of the 80 MHz VCXO in the CMOS molecular clock and the free-running 80 MHz VCXO over a measurement time 4,000 s. The integration time for each frequency point is 1s.

substrate, which can cause tilting of the baseline and drift of the output frequency. This nevertheless does not rule out the feasibility of a single-chip clock in the future. The sub-terahertz signal is generated by a MOSFET-based frequency multiplier chain (×4) fed by a 57.77 GHz phase-locked loop (PLL). An 80 MHz VCXO is used as the input reference of the PLL. Due to the limited maximum oscillation frequency of the silicon MOSFETs ( $f_{\text{max}} \approx 220 \,\text{GHz}$ ), the chip output power decreases rapidly at higher output frequency. Therefore, the OCS spectral line at 231.060983 GHz  $(J=19\leftarrow18)$ , instead of the previously adopted line at 267.530 GHz, is chosen to lower the chip power consumption. The on-chip PLL is equipped with a 40-bit,  $\Delta$ - $\Sigma$  fractional-N modulator, which enables an output frequency-tuning resolution of  $1 \times 10^{-12}$ . The PLL also performs frequency-shift-keying (FSK) modulation for WMS, with an  $f_m$  of 16kHz and  $\Delta f$  of 1MHz. On the Rx side, a MOSFET-based subterahertz square-law power detector, a low-noise operational amplifier (op-amp) and an on-chip lock-in detector are integrated to demodulate the probing sub-terahertz signal. A pair of waveguideto-chip transitions based on a waveguide E-plane quartz probe34 is implemented to connect the CMOS chips with a WR-4.3 waveguide gas cell. The measured output power of the Tx and the noise equivalent power (NEP) of Rx, including ~10 dB loss of each quartz probe, are -20.2 dBm and 0.5 nW Hz<sup>-0.5</sup>, respectively. Figure 5d presents the measured fundamental dispersion curve using the packaged CMOS molecular clock module with an open-loop configuration and an OCS pressure of 5 Pa. A SNR (with 1 Hz bandwidth) of 53 dB is obtained. Next, with a closed-loop configuration, the instantaneous frequency of the clock chip is measured for 4,000 s (Fig. 5f). Compared to a free-running VCXO, although the shortterm stability of the clock is degraded due to its limited SNR, the

long-term stability is improved by ~10 times through locking to the OCS spectral line. Figure 5e presents the measured Allan deviation of the clock, which reaches  $2.4\times10^{-9}$  for  $\tau=1\,\mathrm{s}$  and  $3.8\times10^{-10}$  for  $\tau=1,000\,\mathrm{s}$ , respectively. The CMOS chips consume a total d.c. power of only 66 mW. The total size of the CMOS molecular clock module is 50 cm<sup>3</sup>.

### Conclusion

We have demonstrated a fully-electronic clock using a physical mechanism—sub-terahertz rotational spectroscopy—as an alternative to previous miniature clocks. The Allan deviation results obtained from our lab-scale prototype indicate a stability performance (up to  $\tau = 1,000$  s) comparable with that of CSACs. The clock requires neither an electromagnetic shield nor a gas cell heater, and features instantaneous turn-on operation and wide loop bandwidth. In addition, a chip-scale integration of the molecular clock has also been developed, which effectively reduces the cost, power consumption and size. It is noteworthy that there is still significant room for improving the performance of the CMOS molecular clock. First, most of the 50 cm<sup>3</sup> total volume of the clock package is taken up by vacuum sealing, which can be shrunk. The actual volume enclosed in the meander waveguide cell, which is the ultimate limit for the clock size, is below 100 mm<sup>3</sup>. It is therefore feasible to miniaturize the clock to 1 cm<sup>3</sup> and below. Working with other spectral lines at higher frequencies further reduces the gas cell size. For example, a water ( ${}^{1}H_{2}^{16}O$ ) line at 556.936 GHz ( $J=1 \leftarrow 0$ ) presents 158× stronger integrated absorption intensity<sup>35</sup> than the OCS line  $(J=22\leftarrow21)$  investigated here, and can shrink the gas cell volume by ~200 times. This of course poses more challenges in the electronic design. Second, at present, the SNR of the CMOS molecular ARTICLES NATURE ELECTRONICS

clock is still severely degraded by the noise of the square-law detector, the loss of the waveguide-to-chip transitions (~20 dB in total) and the phase noise of the on-chip PLL. Improved designs of the electromagnetic structures and circuits will bridge the performance gap between the two prototypes shown here. Third, as mentioned earlier (Figs. 4 and 5), the long-term frequency drift causing deviation from the predicted performance is mainly due to the slow gas leakage of our set-up. This problem is expected to be alleviated by a dedicated hermetic package in the future. Stability at the  $1 \times 10^{-12}$ level should then be achievable. Finally, the energy efficiency of the clock can also be enhanced by removing the VCXO, which consumes  $\sim$ 10–20 mW of d.c. power but is only used to ensure that the sub-terahertz probing frequency lies within the molecular spectral line during clock initialization. A crystal-free clock with an alternative on-chip initialization mechanism is expected to reduce the total d.c. power to <40 mW. In summary, the molecular clocks shown in this paper, although still preliminary, provide a promising route towards miniature time-keeping devices that can be monolithically integrated with mainstream CMOS process.

### Methods

Loop bandwidth and settling time of the molecular clock. For our clock with wavelength modulation scheme, to concentrate the spread RF spectrum within the molecular linewidth, the upper limit of the modulation speed  $f_{\rm m}$  should be  ${\sim}0.1\times$ the FWHM. From a physics perspective, the molecules behave as high-Q cavities near resonance, which require a long time for energy charging and discharging via detuning. As a result, the maximum refresh rate for the information of the instantaneous frequency offset is  $f_m$  or 0.1× the FWHM. On the other hand, for a clock control loop with an RC filter (Fig. 3b), the correction speed of the probing frequency (that is, the changing speed of the VCXO control voltage  $V_{xo}$ ) is similar to the closed-loop bandwidth, which is  $f_{BW} = K_v K_r G/(2\pi RC)$ . Because this correction speed cannot exceed the above refresh rate  $f_{\mathrm{m}}$ , the closed-loop bandwidth of the clock is ultimately determined by the absolute spectral linewidth  $(f_{\text{\tiny BW}} < 0.1 \times \text{FWHM})$ . The broader bandwidth leads to faster frequency settling. When the loop bandwidth is much larger than the variation rate of an external disturbance to the clock, the disturbance can be modelled as a step-function voltage  $\Delta V$  added to  $V_{xo}$  at t=0. The response of the clock is then an exponential decay in the time domain:

$$\frac{V_{\rm XO}(t)}{\Delta V} = \frac{1}{K_{\nu}K_{r}G} + e^{\frac{K_{\nu}K_{r}G}{RC}t} \tag{1}$$

with a settling time constant of RC/(K,K,G) or  $1/(2\pi f_{\rm BW})$ . Our laboratory-scale prototype utilizing the 267.530239 GHz ( $J=22\leftarrow21$ ) spectral line has an  $f_{\rm m}$  of 100 kHz, an open-loop gain K,K,G of  $9.3\times10^5$ , and an RC filter cutoff frequency of 0.32 Hz. Thus, the clock bandwidth  $f_{\rm BW}$  is 3.0 kHz, and the settling time constant is  $53\,\mu$ s. Although the current prototype is not optimized for the maximum bandwidth, it is still responsive to disturbances like vibration at the kilohertz level. Crystal oscillators have a shock sensitivity at an approximately ppb per g level of an approximately ppb per g level have indicated that such a disturbance is problematic for CSACs lone fact, given the large linewidth ( $\sim1$  MHz) of the OCS transitions in the subterahertz range, the settling speed of future improved molecular clocks is expected to be  $\sim1,000$  times larger than their caesium counterparts using the 9.192 GHz hyperfine transition (with a linewidth on the order of 1 kHz).

Details of the laboratory-scale molecular clock. The WR-4.3 waveguide gas cell was fabricated with aluminium using computer numerical controlled machining. A total waveguide length of 140 mm was chosen for maximum SNR. The input and output waveguide flanges of the gas cell were sealed with optically transparent epoxy (EPO-TEK 301-2 from Epoxy Technology). The total measured loss of the gas cell was ~7 dB at ~200-270 GHz (4 dB of which is from the epoxy). An OCS gas sample from Sigma-Aldrich was used in the prototype. The gas cell was first evacuated by a turbo vacuum pump (Edwards Vacuum TS75W). The gas sample was then injected with a pressure of 10 Pa. Although a small gas cell was used, the wall broadening determined by the physical dimensions of the gas cell was 71 kHz, which only decreased the quality factor Q by 6% at 10 Pa. The 267.530 GHz signal for spectral-line probing was generated by a WR-3.4 frequency multiplier chain (× 18) (Virginia Diode Inc. (VDI) N5262AW03) driven by a Keysight E8257D signal generator ( $f_{\text{out}} = 14.863 \,\text{GHz}$ ). A WR-3.4 VDI heterodyne receiver (33 dB noise figure) cascaded by an low noise amplifier (Mini-circuits ZX60-6013E-S+), a bandpass filter, a square-law detector (Crystek CPDETLS-4000) and a lock-in amplifier (Stanford Research System SR865A) performed error signal detection. The intermediate signal frequency  $f_{\rm IF}$  from the heterodyne receiver was 950 MHz. The modulation signal ( $f_m = 100 \, \text{kHz}$ ) generated by the SR865A was fed to the

E8257D signal generator. All of the above instruments were referenced to a 10 MHz VCXO (obtained through an 80 MHz Crystek CVHD-950 oscillator with a ÷ 8 frequency divider). The analog output of the lock-in amplifier controlled the VCXO for a negative feedback after the low-pass filtering in an RC filter (C=10μF, R=50 kΩ). The baseband amplification was also provided by the SR865A. The overlapping Allan deviation was measured by a Keysight 53230A frequency counter, which used a 10 MHz rubidium time base (Stanford Research System SR625) as reference. The Allan deviation of the rubidium clock was ~1×10<sup>-12</sup> at  $\tau$ =1,000, which is ~10 times better than our molecular clocks under testing.

Long-term stability analysis. The long-term stability of the clock was determined by the following four drift mechanisms. The first is the drift of the free-running VCXO, which is  $\sim 1 \times 10^{-8}$  for  $\tau = 1,000$  s. The molecular clock presents an openloop gain K,K,G of  $9.3 \times 10^3$ , which suppresses the drift of VCXO to  $1 \times 10^{-11}$ according to equation (2). The second is the pressure/temperature dependency. The pressure variation not only changes the spectral linewidth, but also shifts the centre frequency<sup>25,37</sup>. Our chosen spectral lines ( $J = 22 \leftarrow 21$  and  $J = 19 \leftarrow 18$ ) of OCS have a reported pressure dependency on the order of  $1 \times 10^{-10} \,\mathrm{Pa^{-1}}$  (ref. <sup>37</sup>), which is also observed in our experiments. According to the gas law, this corresponds to a temperature dependency of  $\sim 1 \times 10^{-11} \, \mathrm{K}^{-1}$ . Note that the temperature variation can also directly alter the linewidth and peak absorption intensity due to the velocity dependency of the collisional cross-section; this, however, has much less impact compared to the above pressure-induced effect. The third mechanism is the Zeeman effect. Our probed spectral line contains all sublevels. A magnetic field only causes a  $\sigma$ -component doublet splitting, which is symmetric and should not shift the overall line centre. Even for a conservative estimation, the first-order magnetic-induced shift of one  $\sigma$ -component is only  $\pm 23$  Hz G<sup>-1</sup> (ref. <sup>29</sup>) (or  $8.6 \times 10^{-11}$  G<sup>-1</sup> for the 267.530 GHz line). Thus, no magnetic shield is required for our molecular clock. In comparison, in caesium clocks, even for the (F=4, $m_F = 0$ )  $\rightarrow$  (F = 3,  $m_F = 0$ ) hyperfine transition, which is most insensitive to the magnetic field and has only a second-order magnetic-induced drift, the coefficient is still as high as  $427 \,\text{Hz}\,\text{G}^{-2}$  (or  $4.6 \times 10^{-8}\,\text{G}^{-2}$  at  $9.19 \,\text{GHz}$ )<sup>38</sup>. The fourth mechanism is the Stark effect, where the external electrical field twists the dipole of molecules and leads to asymmetric frequency shifts of the sublevels. The clock RF power is below 100 µW, which is related to a peak electrical field of 835 V m<sup>-1</sup> in the centre of the single-mode waveguide (Fig. 1c). For the chosen OCS spectral line, the calculated largest sublevel Stark shift is  $\sim$ 0.3 Hz. Near the two side walls of the waveguide, the TE<sub>01</sub>-mode wave has zero electrical-field intensity (hence zero Stark shift). Therefore, the upper bound of the systematic frequency offset, due to the stray field, is 0.3 Hz. The RF power of the clock has a fluctuation of ~10%, which leads to a relative drift of only  $1 \times 10^{-13}$ . Thus, no dedicated power stabilization is applied.

**Data availability.** The data that support the plots within this paper and other findings of this study are available from the corresponding author upon reasonable request.

Received: 27 February 2018; Accepted: 15 June 2018; Published online: 13 July 2018

# References

- Audoin, C. & Guinot, B. The Measurement of Time, Frequency and the Atomic Clock (Cambridge Univ. Press, Cambridge, 2001).
- Lombardi, M. A. in *The Mechatronics Handbook* (ed. Bishop, R. H.) Ch. 17 (CRC Press, New York, NY, 2001).
- Nguyen, C. T. C. MEMS technology for timing and frequency control. IEEE Trans. Ultrason. Ferroelectr. Freq. Control. 54, 251–270 (2007).
- Fifty years of atomic time-keeping: 1955 to 2005. Special Issue. Metrologia 42, S1–S156 (2005).
- Lombardi, M. A., Heavner, T. P. & Jefferts, S. R. NIST primary frequency standards and the realization of the SI second. NCSL Int. Meas. 2, 74–89 (2007).
- Lutwak, R. Principles of atomic clocks. In IEEE Int. Frequency Control Symp. (IEEE, 2011).
- Alzetta, G., Gozzini, A., Moi, L. & Orriols, G. An experimental method for the observation of R.F. transitions and laser beat resonances in oriented Na vapour. *Nuovo Cim. B* 36, 5–20 (1976).
- Arimondo, E. & Orriols, G. Nonabsorbing atomic coherences by coherent two-photon transitions in a three-level optical pumping. *Lett. Al Nuovo Cim.* 17, 333–338 (1976).
- Cyr, N., Tetu, M. & Breton, M. All-optical microwave frequency standard: a proposal. IEEE Trans. Instrum. Meas. 42, 640–649 (1993).
- Vanier, J. Atomic clocks based on coherent population trapping: a review. Appl. Phys. B 81, 421–442 (2005).
- 11. Knappe, S. et al. A microfabricated atomic clock. *Appl. Phys. Lett.* **85**, 1460–1462 (2004).
- Lutwak, R. et al. The chip-scale atomic clock—prototype evaluation. In 39th Ann. Precise Time and Time Interval Meeting 269–290 (ION, 2007).

NATURE ELECTRONICS ARTICLES

- 13. Youngner, D. et al. A manufacturable chip-scale atomic clock. In Solid-State Sensors, Actuators and Microsystems Conference 2007, 39–44 (IEEE, 2007).
- 14. DeNatale, J. et al. Compact, low-power chip-scale atomic clock. In *Position, Location and Navigation Symposium 2008*, 67–70 (IEEE, 2008).
- Haesler, J. et al. The integrated Swiss miniature atomic clock. In Joint European Frequency and Time Forum & International Frequency Control Symposium (EFTF/IFC) 2013, 579–581 (IEEE, 2013).
- Quantum SA.45s chip scale atomic clock (Microsemi, 2017); https://www. microsemi.com/document-portal/doc\_download/133305-sa-45s-csac-datasheet
- 17. Riley, W. Handbook of Frequency Stability Analysis (NIST, Gaithersburg, MD, 2008).
- Shock and vibration testing of the SA.45s chip scale atomic clock (CSAC) validation build units (Microsemi, 2014); https://www.microsemi.com/ document-portal/doc\_download/133153-shock-and-vibration-testing-of-thesa-45s-chip-scale-atomic-clock-csac-validation-build-units
- 19. Good, W. E. The inversion spectrum of ammonia. Phys. Rev. 70, 213-218 (1946).
- Smith, W. V., Quevedo, J. L. G. D., Carter, R. L. & Bennett, W. S. Frequency stabilization of microwave oscillators by spectrum lines. *J. Appl. Phys.* 18, 1112–1115 (1947).
- Hershberger, W. D. & Norton, L. E. Frequency stabilization with microwave spectral lines. RCA Rev. 9, 38–49 (1948).
- 22. Townes, C. H. Atomic clocks and frequency stabilization on microwave spectral lines. *J. Appl. Phys.* 22, 1365–1372 (1951).
- Gordon, J. P., Zeiger, H. J. & Townes, C. H. Molecular microwave oscillator and new hyperfine structure in the microwave spectrum of NH<sub>3</sub>. *Phys. Rev.* 95, 282–284 (1954).
- Wineland, H. D. A., David, J. & Hellwig, H. Special purpose atomic (molecular) standard. In Proc. Eighth Annual Precise Time and Material Interval Applications and Planning Meeting 429–448 (IEEE, 1977).
- Townes, C. H. & Schawlow, A. L. Microwave Spectroscopy (Courier Corporation, Chelmsford, MA, 2013).
- Wineland, D. J., Howe, D. A. & Mohler, M. B. Results with the specialpurpose ammonia frequency standard. In 31st Ann. Symp. on Frequency Control 1977, 562–573 (IEEE, 1977).
- 27. Wang, C. & Han, R. Rapid and energy-efficient molecular sensing using dual mm-wave combs in 65 nm CMOS: a 220-to-320 GHz spectrometer with 5.2 mW radiated power and 14.6-to-19.5 dB noise figure. In *International* Solid-State Circuit Conference (ISSCC), 18–20 (IEEE, 2017).
- 28. Ferm, R. J. The chemistry of carbonyl sulfide. Chem. Rev. 57, 621-640 (1957).
- Cox, J. T. & Gordy, W. Zeeman effect of some linear and symmetric-top molecules. *Phys. Rev.* 101, 1298–1304 (1956).
- Vanier, J. & Bernier, L.-G. On the signal-to-noise ratio and short-term stability of passive rubidium frequency standards. *IEEE Trans. Instrum. Meas.* 1001, 277–282 (1981).
- Karplus, R. & Schwinger, J. A note on saturation in microwave spectroscopy. Phys. Rev. 73, 1020–1026 (1948).
- Supplee, J. M., Whittaker, E. A. & Lenth, W. Theoretical description of frequency modulation and wavelength modulation spectroscopy. *Appl. Opt.* 33, 6294–6302 (1994).

- Wang, C. et al. CMOA molecular clock probing 231.061-GHz rotational line of OCS with sub-ppb long-term stability and 66-mW dc power. In 2018 Symp. on VLSI Technology and Circuits (IEEE, 2018).
- 34. Wang, C. et al. Robust sub-harmonic mixer at 340 GHz using intrinsic resonances of hammer-head filter and improved diode model. *J. Infrared Millim. Terahertz Waves* 38, 1397–1415 (2017).
- Jet Propulsion Laboratory molecular spectroscopy catalog; https://spec. ipl.nasa.gov/
- 36. Hati, A., Nelson, C. & Howe, D. in *Aerial Vehicles* 259–286 (In-Tech, Vienna, 2009).
- Koshelev, M. A., Tretyakov, M. Y., Rohart, F. & Bouanich, J.-P. Speed dependence of collisional relaxation in ground vibrational state of OCS: rotational behaviour. J. Chem. Phys. 136, 124316 (2012).
- Yang, S. H., Baek, K. J., Kwon, T. Y., Kim, Y. B. & Lee, H. S. Second-order Zeeman frequency shift in the optically pumped cesium beam frequency standard with a dual servo system. *Jpn J. Appl. Phys.* 38, 6174–6177 (1999).
- 39. GATS, I. Spectral Calculator; http://www.spectralcalc.com

# Acknowledgements

The authors thank S. Coy (MIT, Department of Chemistry), R. Field (MIT, Department of Chemistry), D. Buss (Texas Instruments and MIT, Department of Electrical Engineering and Computer Science), B. Perkins (MIT Lincoln Labs), J. Muenter (University of Rochester, Department of Chemistry) and P. Nadeau (MIT, Department of Electrical Engineering and Computer Science) for helpful technical discussions. The authors also thank Y. Zhang and K. Nelson (MIT, Department of Chemistry) for help with OCS preparation and other technical support. This work was supported by an NSF CAREER award (ECCS-1653100), MIT Lincoln Laboratory, MIT Center of Integrated Circuits and Systems, and a Texas Instrument Fellowship.

### **Author contributions**

C.W. and R.H. conceived and designed the research. C.W. constructed the two prototypes (including the laboratory-scale and chip-scale molecular clocks). X.Y. conducted the design of the VCXO and analysis of the clock-loop dynamics. C.W., M.K. and Z.W. conducted spectroscopy experiments. C.W. and J.M. conducted clock stability characterization. C.W. and R.H. analysed the data and wrote the manuscript. All authors reviewed the manuscript.

# Competing interests

The authors declare no competing interests.

# Additional information

Reprints and permissions information is available at www.nature.com/reprints.

Correspondence and requests for materials should be addressed to R.H.

**Publisher's note:** Springer Nature remains neutral with regard to jurisdictional claims in published maps and institutional affiliations.